Indirect Impact of Atmospheric Aerosols in Idealized Simulations of Convective–Radiative Quasi Equilibrium. Part II: Double-Moment Microphysics

WOJCIECH W. GRABOWSKI AND HUGH MORRISON

National Center for Atmospheric Research, Boulder, Colorado*

(Manuscript received 1 February 2010, in final form 26 November 2010)

ABSTRACT

This paper extends the previous cloud-resolving modeling study concerning the impact of cloud microphysics on convective–radiative quasi equilibrium (CRQE) over a surface with fixed characteristics and prescribed solar input, both mimicking the mean conditions on earth. The current study applies sophisticated double-moment warm-rain and ice microphysics schemes, which allow for a significantly more realistic representation of the impact of aerosols on precipitation processes and on the coupling between clouds and radiative transfer. Two contrasting cloud condensation nuclei (CCN) characteristics are assumed, representing pristine and polluted conditions, as well as contrasting representations of the effects of entrainment and mixing on the mean cloud droplet size. In addition, four sets of sensitivity simulations are also performed with changes that provide a reference for the main simulation set.

As in the previous study, the CRQE mimics the estimates of globally and annually averaged water and energy fluxes across the earth's atmosphere. There are some differences from the previous study, however, consistent with the slightly lower water vapor content in the troposphere and significantly reduced lower-tropospheric cloud fraction in current simulations. There is also a significant reduction of the difference between the pristine and polluted cases, from ~20 to ~4 W m^{-2} at the surface from ~20 to ~9 W m^{-2} at the top of the atmosphere (TOA). The difference between the homogeneous and extremely inhomogeneous mixing scenarios, ~20 W m^{-2} in the previous study, is reduced to a mere 2 (1) W m^{-2} at the surface (TOA). An unexpected difference between the previous and current simulations is the lower Bowen ratio of the surface heat flux, the partitioning of the total flux into sensible and latent components. It is shown that most of the change comes from the difference in the representation of rain evaporation in the subcloud layer in the single- and double-moment microphysics schemes. The difference affects the mean air temperature and humidity near the surface, and thus the Bowen ratio. The differences between the various simulations are discussed, contrasting the process-level approach with the impact of cloud microphysics on the quasi-equilibrium state with a more appropriate system dynamics approach. The key distinction is that the latter includes the interactions among all the processes in the modeled system.

1. Introduction

Representation of clouds and their impact on the solar (shortwave) and earth's thermal (longwave) radiation remains a challenging aspect in modeling climate and climate change (e.g., Solomon et al. 2007). This is because of a complicated and often poorly understood network of forcings and feedbacks linking various physical and chemical processes that affect clouds, and the enormous range of spatial and temporal scales involved. The range spans about nine orders of magnitude, from scales concerning formation of cloud particles (i.e., fraction of a millimeter) to thousands of kilometers characterizing up-to-planetary-scale atmospheric circulations that provide the large-scale destabilization and/or moistening for cloud processes. Although the impact of nucleating aerosols on cloud microphysics has long been appreciated by the cloud physics community (e.g., the differences between clouds developing in maritime and continental environments; Pruppacher and Klett 1997), the way aerosols affect the clouds-in-climate problem through the indirect aerosol effects is far from being understood. In this paper, we follow Grabowski (2006, hereafter G06) and consider the

* The National Center for Atmospheric Research is sponsored by the National Science Foundation.

Corresponding author address: Wojciech W. Grabowski, MMM, NCAR, P.O. Box 3000, Boulder, CO 80307-3000.
E-mail: grabow@ncar.ucar.edu

DOI: 10.1175/2010JCLI3647.1

indirect impact of atmospheric aerosols in a highly idealized problem of convective–radiative quasi equilibrium (CRQE) over a surface representing the mean conditions on earth.

As argued in G06, an important aspect of the indirect aerosol effect is the difference between the impact of cloud microphysical processes on *a single cloud* and the impact on the *ensemble* of clouds [see also discussions in Grabowski et al. (1999); Grabowski and Petch (2009)]. For the climate, the impact of cloud microphysics on a single cloud is irrelevant because what matters is the cumulative impact on many clouds developing over a specific area over some period of time. The key difference between the impact on a single cloud and on the ensemble of clouds is that only the latter includes the interactions between clouds and their environment. Such interactions often obscure the effects of cloud microphysics (Stevens and Feingold 2009). Perhaps a better way to explain the difference between the single-cloud and cloud ensemble paradigms is to consider a specific process (e.g., the cloud microphysics) and to contrast its impact in isolation and the impact when the entire system dynamics are considered—that is, when all interactions (forcings and feedbacks) between clouds and their environment are taken into account. One might refer to these contrasting views as the process-level reasoning versus the system dynamics reasoning. For instance, the discussion in Rosenfeld et al. (2008) illustrates the process-level reasoning because the impact of cloud microphysics is examined without considering the impact of clouds on their environment. Arguably, the CRQE represents the simplest system in which the role of clouds—and the cloud microphysics in particular—can be investigated from the system dynamics point of view.

In CRQE with prescribed surface characteristics, the surface precipitation from an ensemble of clouds can only change if the atmospheric radiative cooling is modified, assuming the Bowen ratio is unchanged.[1] This is because, in the quasi equilibrium, the tropospheric radiative cooling has to be balanced by the total (latent plus sensible) surface heat flux, and the surface precipitation has to be balanced by the surface latent heat flux. It follows that the time- and space-averaged surface precipitation has to be the same regardless of the cloud microphysics if the atmospheric cooling and surface characteristics remain unchanged. From the system dynamics point of view, the same surface precipitation in different aerosol conditions can be obtained by modifications of the cloud field depth or by a shift between warm-rain and ice processes. The mean surface precipitation can change only when the tropospheric radiative cooling is changed (for instance, by modifying the atmospheric water vapor content for the longwave radiation or by changing absorbing constituents for the shortwave radiation) or when the surface energy budget is changed (cf. G06). In the latter case, the surface conditions have to evolve and further impact the evolution of the system, an effect considered neither in G06 nor here.

The main difference between simulations reported here and in G06 is that current simulations apply a significantly more sophisticated cloud microphysics scheme. The scheme allows for a more realistic representation of aerosol impacts on precipitation processes and on the coupling between clouds and radiation. The next section provides specifics of the problem and the numerical model. Model results are presented in section 3. The differences between this study and G06 are discussed in section 4, together with a broader context for the model results. The summary in section 5 concludes the paper.

2. Problem formulation, the model, and modeling setup

As in G06, we consider an idealized problem of CRQE over a surface mimicking the mean earth conditions. The surface temperature, relative humidity (RH), and albedo are taken as 15°C, 85%, and 0.15, respectively.[2] The initial horizontal flow at all levels is 4 m s^{-1}, and it is maintained by relaxing the mean wind profile toward the initial one using a 1-h time scale. Model results are compared to the mean components of the earth energy budget as discussed in Kiehl and Trenberth (1997, hereafter KT97, their Fig. 7 in particular).

The dynamic model, the same as in G06, is a small-scale nonhydrostatic anelastic fluid flow model used as ''superparameterization'' in simulations described in Grabowski and Smolarkiewicz (1999) and Grabowski (2001, 2004) and in cloud simulations described in Morrison and Grabowski (2008b) and in Grabowski et al. (2010). It assumes 2D geometry with a 200-km periodic horizontal domain and a 1-km horizontal grid

[1] For the sake of argument, we assume here that prescribed surface characteristics imply a unique partitioning of the total surface flux into sensible and latent components. This paper will show that such an assumption is not correct because the partitioning also depends on the surface air characteristics, which are affected by the representation of rain evaporation beneath the cloud layer.

[2] Note that the term ''surface RH'' refers to the availability of moisture at the surface and should not be confused with the surface air relative humidity. The surface water vapor mixing ratio used in the latent heat flux formula is given by $\mathrm{RH}_s q_{\mathrm{vs}}(T_s, p_s)$, where RH_s and q_{vs} refer to the surface RH and the saturated water vapor mixing ratio, respectively, at the surface temperature and pressure of T_s and p_s, respectively.

length (note that a 2-km grid length was used in G06). Better vertical resolution is also used because the model applies a stretched grid with 61 levels as in G06, but the model top is at 18 km (it was at 24 km in G06). A gravity wave absorber is used above the 13-km level. In one set of sensitivity simulations, where the surface temperature is increased to represent tropical conditions, the model top is again at 24 km and 81 levels are used (see the discussion later in this section; the absorber in these simulations starts at 18 km). The Monin–Obukhov surface similarity is used to calculate surface fluxes, and a nonlocal boundary layer scheme (e.g., Troen and Mahrt 1986) is applied to represent unresolved transports within the boundary layer.

The main difference between current simulations and G06 is that a sophisticated cloud microphysics scheme is used here. The warm-rain scheme is the double-moment scheme of Morrison and Grabowski (2007, 2008b) with a Khairoutdinov and Kogan (2000) representation of the autoconversion (see Morrison and Grabowski 2007 for details). Ice processes are represented using the double-moment three-variable scheme of Morrison and Grabowski (2008a). In this approach, the ice-particle mass-dimension and projected-area-dimension relationships vary as a function of particle size and rimed mass fraction. The rimed mass fraction is derived locally by separately predicting two ice mixing ratios, that is, the first one representing ice mass acquired through water vapor deposition and the second one through riming. The third ice variable is the number concentration of ice particles. This approach allows for representing in a natural way a gradual transition from small to large ice particles due to growth by water vapor deposition and aggregation, and from unrimed crystals to graupel due to riming. See Morrison and Grabowski (2008a) for details and Slawinska et al. (2009) for an example of the application of the combined warm-rain and ice schemes to the kinematic model simulation of deep organized convection.

Differences between moist convection developing in clean and polluted environments are simulated assuming two contrasting cloud condensation nuclei (CCN) characteristics, referred to as PRISTINE and POLLUTED environments, respectively. The specification of CCN is similar to Morrison and Grabowski (2007). A single-mode lognormal aerosol size distribution is assumed [see Eq. (9) in Morrison and Grabowski 2007]. The mean radius is 0.05 μm, and the geometric standard deviation is 2 (unitless). The soluble fraction as a function of particle volume is 0.5, with the soluble portion of the aerosol consisting of ammonium sulfate. For PRISTINE environments, the total aerosol number concentration is 200 cm^{-3}; for POLLUTED environments, the total number concentration is 2000 cm^{-3}. We assume that the concentration of heterogeneous ice-forming nuclei (IN) is given by Meyers et al. (1992) as a function of ice supersaturation for deposition and condensation-freezing nucleation. Heterogeneous freezing of cloud droplets via immersion freezing is given by the formulation of Bigg (1953) as implemented by Morrison and Grabowski (2008a). The properties of the heterogeneous IN are assumed to be the same in PRISTINE and POLLUTED environments. The effects of clouds on CCN and IN are not considered, and constant background characteristics are applied throughout the simulations.

One of the foci of the discussion in G06 was the impact of the microphysical transformations during entrainment—the homogeneous versus inhomogeneous mixing (cf. Andrejczuk et al. 2009)—on the quasi-equilibrium state in general, and on the amount of solar radiation reaching the surface in particular. However, because of the simplicity of the single-moment bulk warm-rain scheme used in G06, the representation of various mixing scenarios was highly idealized (cf. section 2a therein). The double-moment warm-rain scheme applied here allows for a more realistic representation of the droplet concentration (e.g., relating the concentration to the cloud-base updraft speed) and the change of cloud droplet size due to cloud–environment mixing (see discussion in section 4b in Morrison and Grabowski 2008b). Specifically, various mixing scenarios are obtained by changing a single parameter [α in Eq. (11) in Morrison and Grabowski 2008b]. This parameter controls whether the required evaporation of cloud water is accompanied by the change of droplet concentration, as in the case of the inhomogeneous mixing (i.e., when $0 < \alpha \leq 1$), or whether the concentration does not change, as in the case of the homogeneous mixing (i.e., when $\alpha = 0$). Strictly speaking, the evaporation affected by α should only be due to parameterized subgrid-scale cloud–environment mixing. However, because of the low spatial resolution, the model excludes any subgrid-scale mixing and most of the evaporation near cloud edges comes from numerical diffusion (cf. Grabowski and Smolarkiewicz 1990). Consequently, we apply α to all evaporation predicted by the warm-rain microphysics scheme. It follows that the simulations with various subgrid-scale mixing scenarios most likely overemphasize their impact on the microphysical properties of water clouds. Herein, we will contrast simulations with the homogeneous mixing ($\alpha = 0$) and simulations assuming the extremely inhomogeneous mixing, $\alpha = 1$.

The radiation transfer model, the same as in G06, comes from the National Center for Atmospheric Research (NCAR)'s Community Climate System Model (Kiehl et al. 1994). A diurnal cycle of solar radiation is not considered, the solar constant is reduced to 342 W m^{-2} (i.e., the nominal solar constant averaged over the entire

planet; cf. Fig. 7 in KT97), and a zero zenith angle is assumed. The effective radius of water droplets and ice crystals for the radiation transfer model is diagnosed, applying assumed spectral characteristics and ice-particle mass-dimension and projected-area-dimension relationships, see Morrison and Grabowski (2008a) for details. The effective radii predicted by the double-moment warm-rain and ice microphysics schemes are additionally limited to be between 4 and 20 μm for the water drops and between 10 and 200 μm for the ice crystals. Such limiting is required to avoid unphysical values predicted by the double-moment scheme in grid points with extremely low water or ice mixing ratios and causing problems when passed to the radiation transfer code. In summary, the representation of cloud microphysical processes and the coupling between cloud processes and radiative transfer is significantly more advanced in current simulations than in G06. It should also be pointed out that, as in G06, direct aerosol effects, which can also cause differences between PRISTINE and POLLUTED environments, are not considered.

The simulations assuming both PRISTINE or POLLUTED aerosols and conditions as in G06 will be referred to BASIC (i.e., the surface temperature and surface RH of 15°C and 85%, respectively; and the horizontal wind of 4 m s^{-1}). This set contains four simulations because PRISTINE and POLLUTED were run with either the homogeneous ($\alpha = 0$) or extremely inhomogeneous ($\alpha = 1$) mixing scenarios. In addition to the BASIC set, four additional simulation sets were performed assuming either PRISTINE or POLLUTED aerosol and the homogeneous mixing scenario only ($\alpha = 0$). In the first set, the assumed horizontally averaged wind was increased to 8 m s^{-1}; this set will be referred to as WIND8. In the second set, the surface RH was reduced from 85% to 75%; this set will be referred to as SRH75. The surface wind and surface RH affect the surface heat fluxes, and the impact that these changes have on the quasi-equilibrium state will be compared to the effects of aerosols. In the third additional set, the two-moment rain scheme (where the rain size distribution intercept parameter N_0 evolves with the predicted mixing ratio and number concentration) was replaced by a single-moment scheme that assumes a constant $N_0 = 10^7$ m^{-4}, the same as used in G06 (and close to the standard value for the Marshall–Palmer distribution of 8×10^6 m^{-4}). This set was motivated by a difference between G06 simulations and the BASIC set, and it will be referred to as MARPAL. In the fourth set, the surface temperature was increased to 28°C to make surface conditions similar to those in the tropics; other conditions were kept as in BASIC except for the incoming solar flux, which was also increased to 436 W m^{-2} to be consistent with conditions in the tropics.

TABLE 1. Simulation sets discussed in this paper.

BASIC	Simulations as in G06
WIND8	Horizontal wind increased to 8 m s^{-1}
SRH75	Surface RH reduced to 75%
MARPAL	Fixed intercept for rain, $N_0 = 10^7$ m^{-4}
ST28	Surface temperature increased to 28°C

This set applies 81 levels and the model top is at 24 km; it will be referred to as ST28. The motivation is to increase the cloud-base temperature and thus the depth of the layer in which warm-rain processes operate. Table 1 lists all the simulation sets discussed in this paper.

Because the quasi-equilibrium state from G06 is expected to change little when a different microphysics scheme is applied, simulations in the sets BASIC, WIND8, SRH75, and MARPAL start from the sounding close to that at the end of G06 simulations and are run for an additional 60 days. The ST28 simulations are initiated from the same sounding as in G06 and are run for 90 days. Model data for all simulations are archived every 6 h. Primary model fields (velocity components, temperature, and moisture variables) are archived as instantaneous fields. Fields required for the moisture and energy budgets (surface sensible and latent heat fluxes, latent heating, surface precipitation rate, and radiative fluxes) as well as conditional sampling statistics are archived as averages over all time steps from the previous 6 h. These procedures are exactly as in G06.

3. Results

a. Temperature and moisture profiles

Figure 1 shows the time evolution of the domain-averaged density-weighted temperature ($\int \rho T\, dz / \int \rho\, dz$) and the precipitable water ($\int \rho q_v\, dz$, where q_v is the water vapor mixing ratio) for PRISTINE and POLLUTED BASIC set simulations with the homogeneous mixing scenario. The figure documents that, as expected, the initial sounding is close to the quasi equilibrium, with relatively small changes of the mean temperature and precipitable water occurring during the initial 10 days of the simulations.[3] As in G06, the POLLUTED case features slightly higher precipitable water and almost

[3] It is important to point out that the density-weighted temperature is sensitive to the assumed model top. This explains why the values in Fig. 1 here and in Fig. 1 in G06 differ by about 3 K. When the density-weighted temperature is calculated using model levels up to 13 km, the temperatures here and in G06 differ only by a few tenths of 1 K, in agreement with the temperature profiles discussed later in the paper.

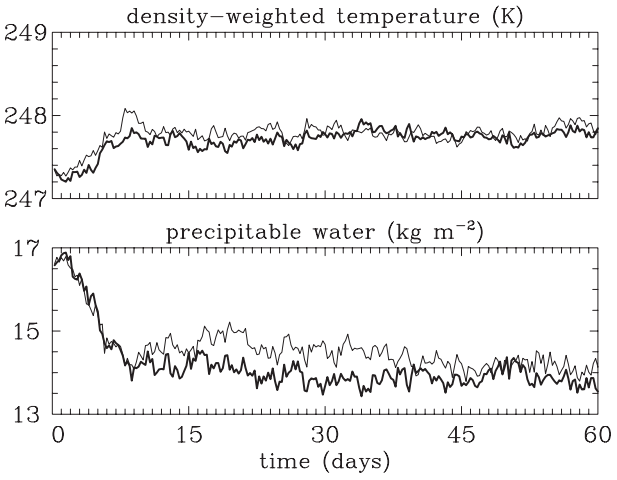

FIG. 1. Evolution of the (top) density-weighted temperature and (bottom) precipitable water for simulations PRISTINE (thick line) and POLLUTED (thin line) with the homogeneous mixing scenario.

the same density-weighted temperature when compared to PRISTINE. The quasi-equilibrium values estimated as averages over the last 30 days are ~247.8 K for the temperature (with the difference between the PRISTINE and POLLUTED cases of 0.03 K) and ~14 kg m^{-2} for the precipitable water (the difference between PRISTINE and POLLUTED is ~0.4 kg m^{-2} or about 3%). The precipitable water is slightly lower than in G06 (14 versus 15 kg m^{-2}), which affects the net surface longwave flux (the greenhouse effect) and the radiative cooling of the troposphere (to be discussed later).

TABLE 2. Density weighted temperature (K, the first number) and precipitable water (kg m^{-2}, the second number) for all simulations discussed in this paper. "BASIC h" and "BASIC ei" refer to the BASIC simulations assuming the homogeneous and extremely inhomogeneous mixing scenarios, respectively.

	PRISTINE	POLLUTED
BASIC h	247.8/13.9	247.8/14.3
BASIC ei	247.8/13.9	247.9/14.3
WIND8	248.6/16.4	248.7/17.0
SRH75	247.0/12.6	247.1/13.0
MARPAL	247.6/14.6	247.7/15.0
ST28	262.0/40.9	262.0/41.6

Table 2 lists the density-weighted temperature and precipitable water for all the simulations presented in this paper. As the table shows, changing the mean wind in the simulation (set WIND8) or modifying the surface RH (set SRH75) has a more significant impact than varying the aerosol characteristics. Precipitable water in MARPAL is close to that in simulations in G06. The set ST28 features significantly higher density-weighted temperature and precipitable water, ~262 K and ~40 kg m^{-2}, respectively, with the PRISTINE simulation featuring ~2% lower precipitable water than the POLLUTED simulation.

The quasi-equilibrium temperature and RH profiles for BASIC PRISTINE and POLLUTED simulations with homogeneous mixing scenario as well as the profiles from G06 simulations (i.e., the initial profiles for current simulations) are shown in Fig. 2. In agreement with the results shown in Fig. 1, the differences between the two simulations and the simulations of G06 are small. The temperature difference between POLLUTED and

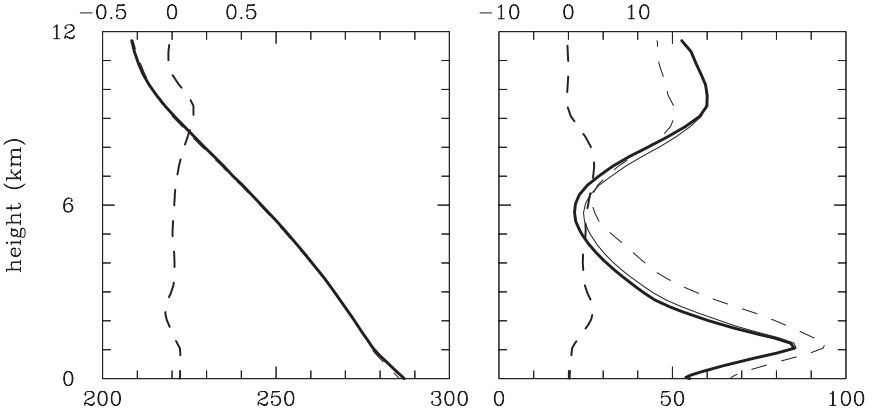

FIG. 2. (left) Quasi-equilibrium temperature and (right) RH profiles for simulations PRISTINE (thick line) and POLLUTED (thin line) with the homogeneous mixing scenario. Initial profiles taken from the simulations discussed in G06 are shown by thin dashed lines (note that the G06 temperature profile is not visible in (left), as all 3 profiles differ less than the thickness of the line). POLLUTED minus PRISTINE differences are shown using the thick dashed lines in the left side of both panels, with the scales provided above each panel.

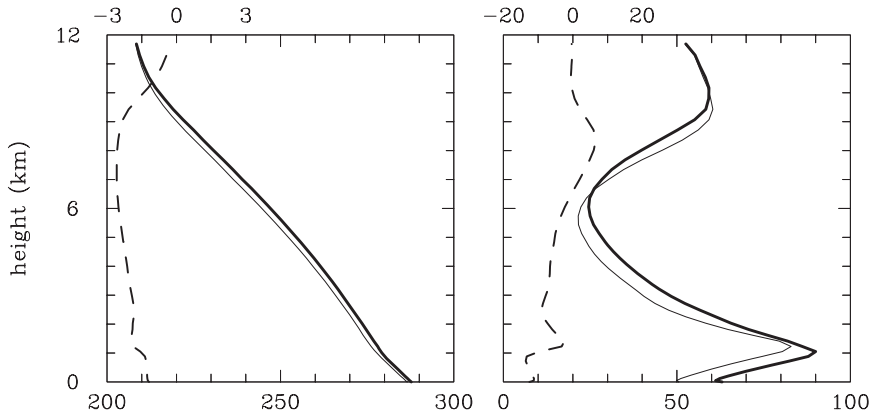

FIG. 3. As in Fig. 2, but comparing profiles for PRISTINE simulations with homogeneous mixing from sets WIND8 (thick line) and SRH75 (thin line). Note the different scales for the SRH75 minus WIND8 differences (shown as dashed lines) when compared to Fig. 2. G06 profiles are not shown.

PRISTINE is smaller than in G06 (a few tenths of 1 K) and—in contrast with G06—the difference is largest in the upper troposphere. As in G06, the RH profiles in PRISTINE and POLLUTED differ by a few percent, and the differences extend into the upper troposphere. The overall shape of RH profiles, with the maximum near the top of the boundary layer and in the upper troposphere, remains similar. The mean surface air temperature is higher than in G06 (13.7° versus 12.3°C in G06), and the water vapor mixing ratio of the surface air is slightly lower (5.5 versus 6.0 g kg^{-1} in G06). These changes are responsible for the differences in the surface Bowen ratio between the simulations presented here and those in G06, as discussed later in the paper. The differences between the POLLUTED and PRISTINE simulations from the BASIC set are small, ~0.05°C for the surface temperature and 0.03 g kg^{-1} for the water vapor mixing ratio. The results for BASIC simulations with extremely inhomogeneous mixing are similar to those in Fig. 2 and are not shown.

To put the differences between the POLLUTED and PRISTINE simulations from the BASIC set into

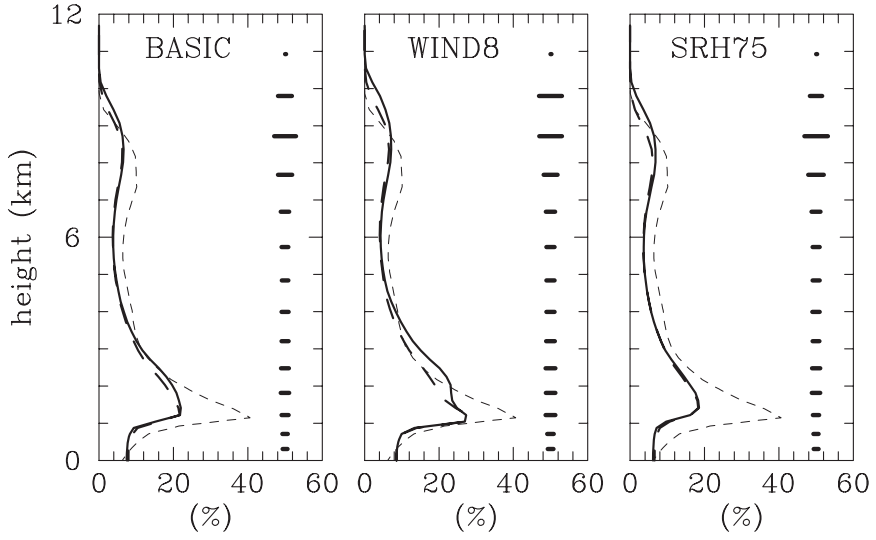

FIG. 4. Quasi-equilibrium profiles of the cloud fraction for simulations POLLUTED (thick solid line) and PRISTINE (thick dashed line) with the homogeneous mixing scenario in BASIC, WIND8, and SRH75. Thin dashed line shows the profile from the PRISTINE homogeneous mixing case of G06. Length of horizontal bars on the right-hand side of each panel represents the averaged standard deviation (i.e., the mean of the POLLUTED and PRISTINE) of the temporal evolution of the domain mean. Bars are shown only at selected levels.

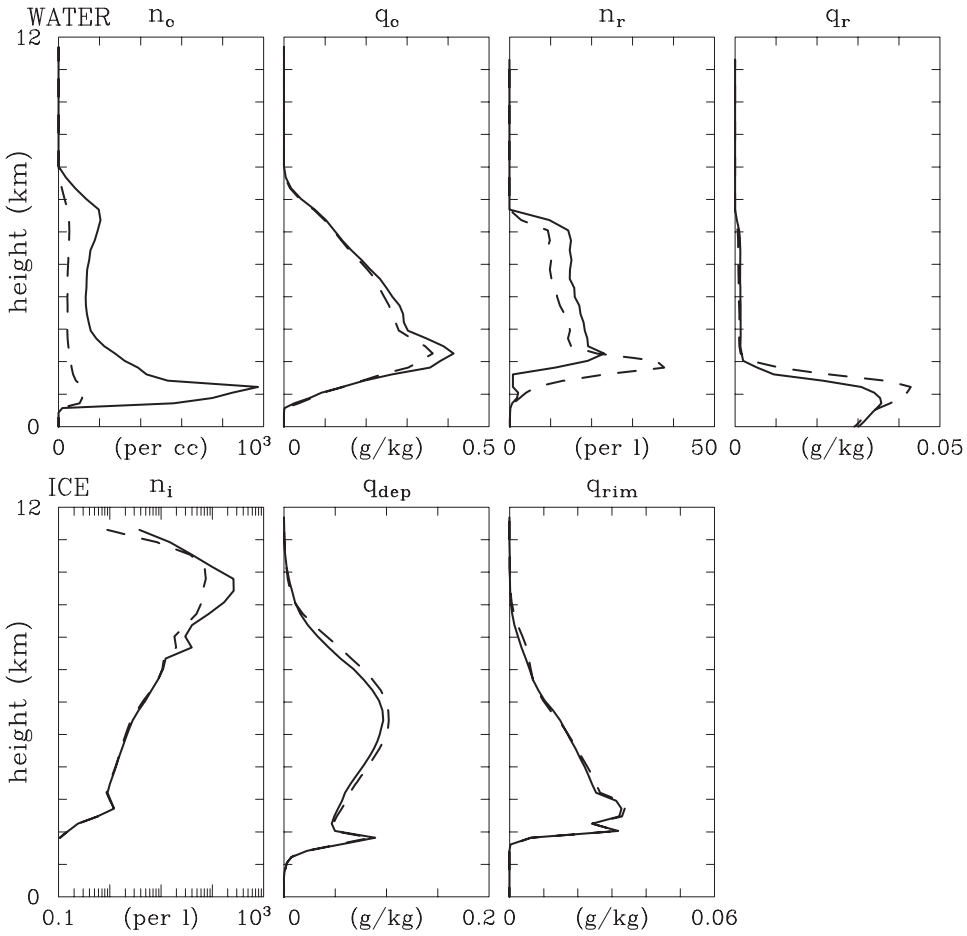

FIG. 5. Quasi-equilibrium profiles of conditionally sampled microphysical fields for POLLUTED (solid line) and PRISTINE (dashed line) BASIC simulations with the homogeneous mixing scenario: (top) water and (bottom) ice. See text for details.

perspective, Fig. 3 compares quasi-equilibrium profiles from PRISTINE WIND8 and SRH75 simulations (profiles from POLLUTED WIND8 and SRH75 simulations and their differences are similar to those in Fig. 3 and are not shown). As the figure illustrates, reducing the surface RH leads to lower (higher) RH in the lower (upper) half of the troposphere (by 5%–10%) and significantly colder (~2 K) troposphere compared with the WIND8 simulation. Surface air temperature in WIND8 is higher than in SRH75 (14.5° versus 13.3°C) and so is the water vapor mixing ratio of the surface air (6.5 versus 4.8 g kg^{-1}). The key point is that these differences are much larger than those between the BASIC POLLUTED and PRISTINE simulations.

b. Clouds and precipitation

Figure 4 shows quasi-equilibrium (days 31–60) profiles of cloud fraction (defined at any level as the fraction of model grid boxes with a total—cloud plus precipitation—mixing ratio larger than 0.01 g kg^{-1}) for PRISTINE and POLLUTED simulations from the BASIC homogeneous mixing set, as well as sets WIND8 and SRH75.[4] Profiles from the PRISTINE homogeneous mixing case from G06 are also shown for reference. In general, the cloud fraction profiles are similar to those in G06 (i.e., they all feature maxima in the lower and upper troposphere), but the lower-tropospheric cloud fraction is significantly smaller than in G06 (e.g., 22% in BASIC compared with 40% in G06). In all three sets, the PRISTINE case features slightly lower cloud fraction than the POLLUTED case, but the difference in each set is smaller than the differences between all the

[4] Note that only cloud condensate was used in G06 to define cloud fraction. Since the new ice microphysics scheme does not distinguish between cloud and precipitation ice, total condensate is now used to define the cloud fraction. Note that G06 results shown use the modified definition.

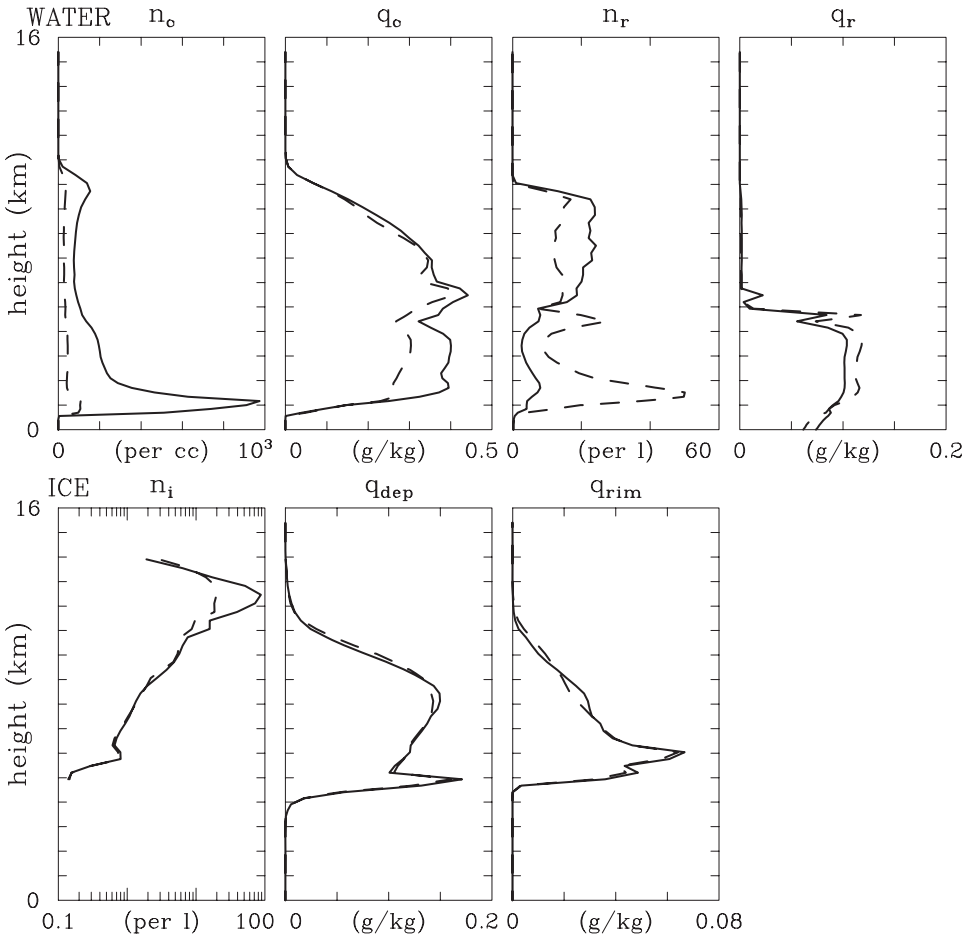

FIG. 6. As in Fig. 5, but for set ST28.

sets. The latter is consistent with the process-level reasoning: increasing surface winds should lead to higher surface latent fluxes and thus to higher lower-tropospheric cloud fraction, whereas reducing surface humidity should have the opposite effect. Such reasoning will be contrasted with the CRQE results (i.e., the system dynamics reasoning) later in the paper. Note that, as in G06, the differences between the PRISTINE and POLLUTED simulations in all the sets are smaller than the temporal variability.

Figures 5 and 6 show profiles of conditionally averaged microphysical properties for PRISTINE and POLLUTED BASIC simulations with homogeneous mixing and from the set ST28, respectively. Conditional sampling of cloud droplet mixing ratio q_c and number concentration n_c includes only points with q_c larger than 0.01 g kg^{-1}; raindrop mixing ratio q_r and number concentration n_r are averaged only for points with q_r larger than 0.001 g kg^{-1}; and ice mixing ratio grown by diffusion of water vapor $q_{\rm dep}$ and by riming $q_{\rm rim}$, and the ice concentration n_i are sampled for points where the total ice mixing ratio $q_{\rm dep} + q_{\rm rim}$ is larger than 0.001 g kg^{-1}. The averages are taken over days 31–60 for BASIC and 46–90 for ST28. For the BASIC set (Fig. 5), the difference in CCN between the PRISTINE and POLLUTED simulations leads to a significant difference in n_c. At the process level, this arguably leads to a significant difference in the conversion of cloud water into rain and results in higher (lower) q_r (q_c) below the melting level (located at ~2 km; cf. Fig. 2). The differences in the ice field are rather small, except for the ice crystal concentration n_i in the upper-tropospheric anvils.

The relatively shallow depth of the layer between the cloud base and the freezing layer in BASIC motivated the simulations in the set ST28. Mean microphysical profiles from this set are shown in Fig. 6. The difference in n_c is similar to BASIC. The differences in q_c and q_r are similar to BASIC as well, with higher (lower) q_r (q_c) below the melting level (located at ~4.5 km). Similarly to BASIC, the difference in q_r profiles between PRISTINE and POLLUTED (and also in n_r profiles; not apparent in the figures) reverses near the surface and leads to

TABLE 3. Energy fluxes in PRISTINE and POLLUTED simulations from the BASIC set with homogeneous and extremely inhomogeneous mixing scenarios. Values in the parentheses show the standard deviations of the temporal evolution.. Estimates of the global-mean energy budgets from KT97 are shown in the last column.

	PRISTINE h	PRISTINE ei	POLLUTED h	POLLUTED ei	KT97
Net TOA shortwave flux (W m^{-2})	256 (3)	257 (3)	247 (4)	248 (5)	235
G06 results	225 (12)	245 (6)	201 (10)	225 (9)	
TOA albedo	0.25 (0.01)	0.25 (0.01)	0.28 (0.01)	0.27 (0.01)	0.31
G06 results	0.34 (0.03)	0.28 (0.03)	0.41 (0.03)	0.34 (0.03)	
OLR (W m^{-2})	251 (4)	252 (4)	247 (8)	246 (12)	235
G06 results	242 (3)	243 (3)	240 (3)	242 (3)	
Radiative cooling of troposphere (W m^{-2})	−94 (4)	−94 (4)	−93 (8)	−91 (12)	−102
G06 results	−101 (4)	−100 (5)	−101 (4)	−99 (4)	
Solar flux absorbed at surface (W m^{-2})	202 (4)	204 (3)	193 (5)	194 (6)	168
G06 results	163 (11)	184 (8)	141 (12)	164 (10)	
Surface net longwave (W m^{-2}) radiation	96 (2)	96 (2)	93 (3)	93 (3)	66
G06 results	73 (5)	73 (6)	70 (5)	73 (5)	
Surface sensible heat flux (W m^{-2})	10 (1)	10 (1)	9 (1)	9 (1)	24
G06 results	20 (2)	20 (1)	19 (1)	18 (2)	
Surface latent heat flux (W m^{-2})	84 (1)	84 (1)	82 (1)	81 (1)	78
G06 results	73 (2)	73 (2)	75 (2)	74 (2)	
Surface precipitation (W m^{-2})	83 (19)	83 (21)	82 (20)	81 (20)	78
G06 results	69 (33)	70 (29)	72 (28)	70 (32)	
Surface energy budget (W m^{-2})	13 (3)	15 (3)	9 (4)	11 (5)	0
G06 results	*−2 (7)*	*17 (5)*	*−23 (9)*	*−2 (7)*	

surface q_r and n_r values smaller for PRISTINE than for POLLUTED. The reason for such a change is related to the representation of the rain evaporation in the double-moment scheme, with larger n_r for PRISTINE above the cloud base leading to a smaller mean drop size and thus more rapid evaporation below the cloud base. This highlights the basic feature of the double-moment scheme where the same precipitation rate (see Tables 3–5 to be discussed in the next section) can be associated with different combinations of q_r and n_r values. The differences in the ice characteristics are also small, except for the ice concentration n_i in the upper troposphere, as in BASIC. Overall, neither Fig. 5 nor Fig. 6 supports the conjecture of Rosenfeld et al. (2008) that the modification of the CCN should result in profound changes of precipitation processes and in the ice field aloft (e.g., the cloud fraction). The rather small differences in microphysical properties between PRISTINE and POLLUTED in BASIC and ST28 suggest that the process-level reasoning exaggerates the role of cloud microphysics when compared with their role in the system dynamics approach.

c. Energy and water fluxes

The key results of this study are summarized in Tables 3–5. The tables present water and energy fluxes

TABLE 4. As in Table 3, but for PRISTINE and POLLUTED simulations from WIND8, SRH75, and MARPAL. Results from G06 are not shown.

	WIND8 PRISTINE	WIND8 POLLUTED	SRH75 PRISTINE	SRH75 POLLUTED	MARPAL PRISTINE	MARPAL POLLUTED	KT97
Net TOA							
Shortwave flux (W m^{-2})	249 (4)	236 (5)	262 (3)	256 (5)	245 (4)	238 (5)	235
TOA albedo	0.27 (0.01)	0.31 (0.01)	0.24 (0.01)	0.25 (0.01)	0.28 (0.01)	0.30 (0.01)	0.31
OLR (W m^{-2})	249 (4)	242 (11)	253 (4)	249 (10)	249 (3)	245 (7)	235
Radiative cooling of troposphere (W m^{-2})	−105 (4)	−101 (12)	−88 (4)	−86 (9)	−97 (3)	−95 (7)	−102
Solar flux absorbed at surface (W m^{-2})	192 (4)	179 (6)	210 (4)	205 (5)	189 (5)	182 (5)	168
Surface net longwave (W m^{-2}) radiation	80 (3)	76 (3)	105 (3)	103 (3)	87 (3)	86 (3)	66
Surface sensible heat flux (W m^{-2})	5 (1)	4 (1)	14 (1)	13 (1)	18 (1)	17 (1)	24
Surface latent heat flux (W m^{-2})	99 (2)	97 (2)	73 (1)	71 (1)	78 (2)	77 (2)	78
Surface precipitation (W m^{-2})	99 (22)	96 (26)	72 (19)	71 (22)	77 (21)	75 (23)	78
Surface energy budget (W m^{-2})	8 (3)	1 (4)	18 (3)	17 (4)	6 (3)	2 (4)	0

TABLE 5. As in Tables 3 and 4, but for PRISTINE and POLLUTED simulations from ST28.

	PRISTINE	POLLUTED
Net TOA shortwave flux (W m^{-2})	331 (3)	323 (4)
TOA albedo	0.23 (0.01)	0.25 (0.01)
OLR (W m^{-2})	290 (4)	288 (6)
Radiative cooling of troposphere (W m^{-2})	−133 (4)	−131 (7)
Solar flux absorbed at surface (W m^{-2})	249 (4)	241 (5)
Surface net longwave (W m^{-2}) radiation	65 (2)	64 (1)
Surface sensible heat flux (W m^{-2})	4 (1)	4 (1)
Surface latent heat flux (W m^{-2})	128 (2)	127 (2)
Surface precipitation (W m^{-2})	127 (45)	126 (45)
Surface energy budget (W m^{-2})	52 (4)	47 (5)

as simulated in cases PRISTINE and POLLUTED from all the sets, in the same format as Table 2 in G06, and compare the fluxes to the diagnosed fluxes in KT97 (except for ST28, in which case the estimates of KT97 are irrelevant). Table 3 also shows corresponding results from G06. In general, results from sets with setups similar to G06 (i.e., these presented in Tables 3 and 4) are consistent with G06, although there are significant differences. Perhaps the most important difference between results from various simulations in the BASIC set (i.e., Table 3) and those in G06 is a large reduction of the spread in the net surface energy flux (referred to in the subsequent discussion as the surface energy budget; cf. G06): a few W m^{-2} versus 20 W m^{-2} or more in G06. The differences between PRISTINE and POLLUTED simulations with the same mixing scenario are ~4 W m^{-2}, and the differences between various mixing scenarios for the same aerosol characteristics are ~2 W m^{-2}. The top-of-the-atmosphere (TOA) net shortwave fluxes differ by a mere 1 W m^{-2} for simulations with different mixing scenarios and the same aerosol characteristics. This is in a dramatic contrast with G06, where corresponding differences were ~20 W m^{-2}. Since the difference between PRISTINE and POLLUTED as well as the difference between various mixing scenarios should (to the first approximation) linearly scale with the low-level cloud fraction, some reductions compared to G06 are anticipated. However, the reductions are significantly larger than the decrease of the lower-tropospheric cloud fractions between G06 and BASIC. The time-averaged TOA albedos are smaller in the BASIC than in G06 (0.26 versus 0.34), most likely because of the smaller lower-tropospheric cloud fraction (cf. Fig. 4). The mean longwave flux at the surface is larger here (96 and 93 W m^{-2} for PRISTINE and POLLUTED, respectively) than in G06 (73 and 70 W m^{-2} for PRISTINE and POLLUTED, respectively) because of the smaller water vapor content in the troposphere (cf. Fig. 1 here and Fig. 1 in G06). The latter is also responsible for a slightly smaller radiative cooling of the troposphere in BASIC, with the average radiative cooling of −93 W m^{-2} among all BASIC simulations versus −100 W m^{-2} in G06. All these changes make the surface energy budgets positive in BASIC simulations, in contrast with negative values in most simulations of G06. An unexpected difference is in the Bowen ratio of the surface flux (i.e., the ratio between sensible and latent fluxes), which was ~0.25 in G06 and is ~0.12 here. Since the surface latent heat flux has to be balanced by the surface precipitation, the hydrological cycle operates ~10% faster in BASIC than in G06. Reasons for the change of the Bowen ratio are explained by the simulation MARPAL that will be discussed shortly. Note that the higher surface precipitation rate and the smaller lower-tropospheric cloud fraction in BASIC compared with G06 is accompanied by the decreased tropospheric water vapor content. This can be interpreted as higher precipitation efficiency and reduced cloud detrainment in current simulations.

Table 4, in the format of Table 3, documents results from simulations WIND8, SRH75, and MARPAL. Increasing the mean wind in WIND8 leads to an increase of the total surface flux, higher precipitable water (cf. Table 2), larger tropospheric cooling, larger TOA albedo (related to larger lower-tropospheric cloud fraction; cf. Fig. 4), larger difference between PRISTINE and POLLUTED (13 W m^{-2} at TOA and 7 W m^{-2} at the surface), and faster hydrological cycle (i.e., larger surface precipitation). The Bowen ratio is even smaller (0.05). Note that, in the quasi equilibrium, an increase of the surface winds *does not* have to lead to the increase of the total surface heat flux. For instance, if the radiative cooling of the troposphere remained unchanged between BASIC and WIND8, the surface heat flux would have to remain constant. Stronger surface winds would then have to be compensated by a reduction of the temperature and water vapor difference between the surface and the near-surface air so that the surface heat flux remained unchanged. The surface flux in WIND8 is larger only because these simulations feature larger tropospheric radiative cooling. If the change of the wind resulted in the reduction of the tropospheric cooling, then the surface flux would have to decrease. In other words, the increase of the surface flux is a result of the feedback between radiative cooling and convection, with the stronger radiative cooling resulting from the higher tropospheric water vapor content for WIND8 (Table 2).

Comparing surface fluxes in BASIC and WIND8 leads to the following observation, highlighting the difference between the process-level reasoning and the system

dynamics reasoning. In the case of the total surface heat flux, the process-level reasoning (i.e., stronger winds leading to the larger total surface flux) agrees with the system dynamics reasoning because stronger radiative cooling is accompanied by larger surface heat fluxes in this case. However, the increase of the total surface heat flux between BASIC and WIND8 dictated by the increase of the radiative cooling (~12%) is far less than dictated by the surface wind increase (~80%; not shown). At the same time, the surface sensible heat flux is reduced, from ~10 W m^{-2} in BASIC to ~5 W m^{-2} in WIND8. In this case, the process-level reasoning implies an increase of the surface sensible flux (because of the increase of surface wind), in contrast with what the system dynamics results produce.

A similar argument can be used to explain the results from SRH75 in Table 4. Reducing the surface RH in SRH75 results in lower TOA albedo (because of the smaller lower-tropospheric cloud fraction; this also leads to a larger solar flux absorbed at the surface) and smaller tropospheric cooling (because of the reduced water vapor content, cf. Table 2). The latter requires a smaller total surface heat flux and, since the surface RH is smaller than in BASIC and WIND8, the Bowen ratio is larger. Note that the process-level reasoning applied to the surface sensible heat flux again leads to a mistake, as neither the surface temperature nor the mean surface wind changed but the surface sensible flux increased.

Replacing the two-moment scheme for rain (where rain intercept parameter N_0 evolves in space and time) with the fixed-intercept Marshall–Palmer formulation of the raindrop spectra (set MARPAL) results in the Bowen ratio close to that in G06 (cf. our Table 4 with Table 3 in G06). Results from MARPAL suggest an explanation for the simulated change of the Bowen ratio between G06 and BASIC. As noted above, in quasi equilibrium, the total surface heat flux balances the radiative cooling of the troposphere. Since tropospheric cooling changes by a few W m^{-2} between simulations in G06 and in BASIC and MARPAL, the total surface flux has to be approximately the same. However, the partitioning between the sensible and latent flux components can be different. The smaller Bowen ratio in BASIC is consistent with warmer air temperature and lower water vapor mixing near the surface, as pointed out when discussing Fig. 2. Figure 7 shows the potential temperature profiles near the surface in PRISTINE homogeneous mixing from G06, BASIC, and MARPAL. The profiles are derived as either the domain averages (dashed lines) or using only points with significant rain ($q_r > 10^{-4}$ kg kg^{-1}; solid lines). The motivation for such an analysis is as follows. Precipitation (rain in particular) is typically accompanied by a subsiding motion—that is, either convective or mesoscale downdraft. Such a downdraft is driven by both loading and evaporation of precipitation and supplies the boundary layer (surface layer in particular) with air of low equivalent potential temperature (i.e., relatively cold and dry). In convective situations, the precipitation-laden downdrafts result in the so-called cold pools in the boundary layer, which play an important role in the surface–atmosphere exchange.

As Fig. 7 shows, the simulation reported in G06 features near-surface air in raining regions on average 5 K colder than the surface. This results in the average surface temperature difference (between the surface and the air near the surface; dashed line) of ~2 K. Conversely, in the BASIC simulation, the temperature profile in raining regions is closer to the dry adiabatic, and the surface temperature difference is only ~2.5 K. This leads to a significantly lower average temperature difference and thus smaller mean sensible heat flux. When a fixed-intercept Marshall–Palmer distribution of raindrops is assumed in the simulation MARPAL (10^7 m^{-4}), the results near the surface are much closer to the G06 simulation: the temperature gradient is closer to the gradient in G06, and the mean temperature difference is only slightly smaller than in G06. The explanation for these results is that the evaporation rate of falling rain in G06 (where Marshall–Palmer raindrop size distribution is assumed) and MARPAL is different than in BASIC (where the intercept parameter of the raindrop distribution is allowed to evolve). The intercept parameter predicted by the double-moment scheme in BASIC is ~10^6 m^{-4} in the lowest few hundred meters near the surface (not shown)—that is, an order magnitude smaller than assumed in MARPAL. This implies the presence of larger raindrops that evaporate slowly as they fall through the boundary layer and thus a closer-to-dry adiabatic temperature lapse rate in the raining areas near the surface in BASIC. It follows that the difference in the representation of rain evaporation in the simulations in G06 and in BASIC has a profound impact on the partitioning between the sensible and latent components of the surface heat flux.

Finally, Table 5 (in the format of Tables 3 and 4) shows results from the set ST28. The difference between PRISTINE and POLLUTED are again relatively small: the TOA albedo differs by 0.02, and most of the fluxes differ by a few watts per square meters. The surface energy budget is 52 and 47 W m^{-2} in the PRISTINE and POLLUTED simulations, respectively, which implies that the surface temperature should increase. However, the simulations exclude any large-scale forcing (e.g., because of the large-scale circulation and/or wave activity; Grabowski et al. 1996, 1998; Wu et al. 1998, 1999; Wu and Moncrieff 1999). Including effects of the large-scale

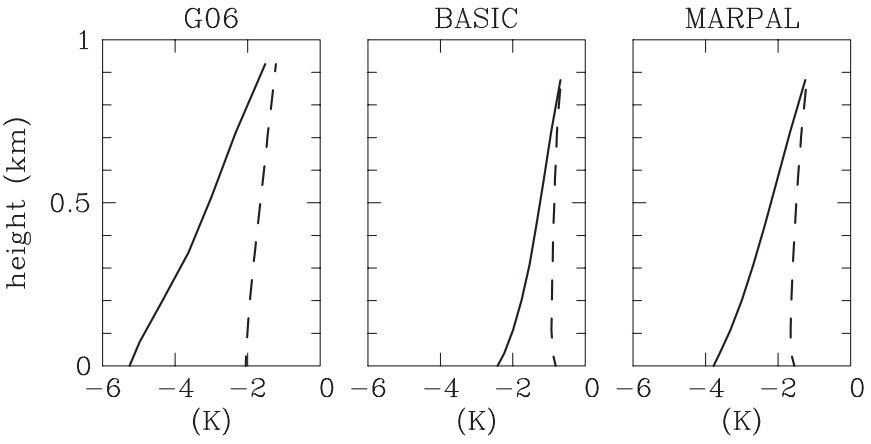

FIG. 7. Potential temperature profiles in the lowest kilometer of the simulation domain shown as deviations from the surface temperature for PRISTINE simulations with the homogeneous mixing discussed in G06 and in similar simulations from the BASIC and MARPAL sets. Solid lines represent profiles sampled over grid points with rain, whereas dashed lines are for domain-averaged profiles.

forcing would arguably increase cloudiness and thus the TOA albedo, and reduce the surface warming implied by the positive surface energy budget.

4. Discussion

a. Differences between BASIC simulations and G06

The main differences between G06 and current simulations are as follows: (i) the smaller lower-tropospheric cloud fraction, which affects the mean TOA albedo and the surface energy budget; (ii) the smaller total water vapor content in the troposphere, which affects TOA outgoing longwave radiation (OLR) and the mean radiative cooling of the troposphere; (iii) the smaller difference in the net surface energy flux between the PRISTINE and POLLUTED conditions and the very small (perhaps insignificant) impact of various mixing scenarios; and (iv) the significantly reduced Bowen ratio of the surface flux.

As hinted in the previous section, the change of the lower-tropospheric cloud fraction and precipitable water can be interpreted as the impact of higher precipitation efficiency and smaller detrainment in the current simulations. Since the simulations in G06 featured lower spatial resolution, one may wonder if the horizontal gridlength change can explain the differences. To quantify this issue, we reran the BASIC simulations, applying the 2-km horizontal grid length as in G06. The results suggest that the horizontal resolution change can explain some but not all the differences. For instance, the lower-tropospheric cloud fraction increased in 2-km simulations to ~25% (from 22% in BASIC) compared with ~40% in G06. The precipitable water increased to 14.6 and 14.9 kg m^{-2} (from 13.9 and 14.3 kg m^{-2} in BASIC) compared with 15.3 and 15.6 kg m^{-2} in G06 for PRISTINE and POLLUTED conditions, respectively.

The smaller difference in the net surface energy flux between PRISTINE and POLLUTED and the insignificant impact of various mixing scenarios in current simulations highlight the simplicity of the approach used in G06. The microphysics scheme (Grabowski 1998) was extremely simple in G06, assuming the temperature-dependent partitioning of the cloud condensate (between cloud water and cloud ice) and precipitation (between rain and snow), and applying saturation adjustment (with water–ice saturation in warm–cold conditions and a linear transition between the two) to locally evolve the cloud condensate mixing ratio. This is in dramatic contrast with the double-moment scheme used here, which predicts mixing ratios and concentrations of liquid and solid cloud and precipitation particles, and attempts to represent the impacts of various particle formation and growth mechanisms on the spatial and temporal evolution of cloud microphysical properties. In contrast, G06 had to use additional assumptions to locally diagnose the droplet mean volume radius and thus the effective radius for the radiative transfer. The effective radius of the ice field was diagnosed based on the local ice mixing ratio alone. As far as the homogeneity of subgrid-scale mixing of warm clouds is concerned, the differences between homogeneous and extremely inhomogeneous mixing are represented in the double-moment scheme in a realistic way using predicted droplet concentration and its changes during evaporation [e.g., Eq. (11) in Morrison and Grabowski 2008b]. In contrast, the homogeneity of mixing in G06 was considered in a very

idealized way. For the homogeneous mixing case, G06 simply assumed that the droplet concentration could be taken as 100 (1000) cm^{-1} in PRISTINE (POLLUTED) and that the dilution effect could be neglected (see the footnote on p. 4667 in G06). For the extremely inhomogeneous mixing, the local mean volume radius was taken as the radius within an adiabatic air parcel rising from the cloud base with a droplet concentration of 100 (1000) cm^{-1} for PRISTINE (POLLUTED) conditions. The large differences in impact of the mixing scenario between BASIC and G06 suggest the importance of its parameterization in terms of the level of complexity. However, although the impact of the mixing scenario seems insignificant in the current simulations, one needs to keep in mind the rather low spatial resolution of current and G06 simulations, especially for shallow convection for which large-eddy simulation provides a more appropriate framework (cf., Slawinska et al. 2008).

Precipitation formation processes are also significantly more realistic in the microphysics scheme used here (Morrison and Grabowski 2007, 2008a,b) than in Grabowski (1998). As argued above, this has some impact on the results, especially on the low-level cloud fraction and the tropospheric water vapor. However, the differences between the PRISTINE and POLLUTED surface precipitation rates are as small as in G06 because they are controlled by the differences in the atmospheric radiative cooling and Bowen ratio, which are practically the same among all BASIC simulations.

Finally, the differences in the surface flux Bowen ratio between G06 and the current results highlight the role of rain evaporation below the cloud base and its effect on the thermodynamic properties of the air near the surface and thus on the surface fluxes. This impact is similar to that in Morrison et al. (2009), where simulations of the organized convection applying single- and double-moment microphysics were compared. The Bowen ratio obtained in the current simulations is also significantly smaller than in KT97. The Bowen ratio can be compared to the observations and cloud-resolving simulations of tropical oceanic convection and midlatitude summertime continental convection, keeping in mind the higher (lower) surface RH for the ocean (land). For instance, simulations of the Global Atmospheric Research Program (GARP) Atlantic Tropical Experiment (GATE) convection in Grabowski et al. (1998) applying a single-moment warm-rain microphysics scheme showed a significant overestimation of the surface sensible heat flux when compared with the observations (e.g., 20–25 W m^{-2} in the model versus ~10 W m^{-2} in the observations, see Figs. 10 and 11 therein). In Tropical Ocean and Global Atmosphere Coupled Ocean–Atmosphere Response Experiment (TOGA COARE) simulations applying the same model (Wu et al. 1998, 1999), the surface Bowen ratio was ~0.1 and compared relatively well with the observations (e.g., Figs. 10 and 11 in Wu et al. 1998; Table 2 in Wu et al. 1999). Over the midlatitude summertime continents, the Bowen ratio is typically significantly higher, typically between 0.3 and 0.5 (e.g., refer to Table 6 in Xu et al. 2002 for the deep convection Atmospheric Radiation Measurement Program (ARM) case of the U.S. Department of Energy; Fig. 3 in Brown et al. 2002 for the shallow convection; the appendix in Grabowski et al. 2006 for the Amazon convection). Arguably, more detailed comparisons between the simulated and observed partitioning of the surface flux between the sensible and latent components and direct comparison with raindrop size distributions from a disdrometer is needed to investigate this issue in more detail and to provide observational support for the results obtained with the double-moment warm-rain microphysics.

b. *Relevance to the earth climate system*

The 2D small-domain CRQE simulations discussed here and in G06 represent a dramatic simplification of the earth's climate system. For one, the earth's climate involves not only vertical energy fluxes as simulated here but also energy fluxes that have a significant mean horizontal component in the midlatitudes. This is because horizontal poleward transport is needed to balance the mean (shortwave plus longwave) TOA radiative flux difference between low and high latitudes. The horizontal atmospheric component involves baroclinic waves with their frontal systems and accompanying energy and water transports. There is no doubt that frontal clouds play a significant role in the atmospheric radiative transfer and in the hydrological cycle, an aspect excluded from the current study.

Because the computational domain is small and the assumed background horizontal flow is uniform in height, current simulations also exclude the effects of aerosols on organized convection. Although not discussed here (nor in G06), convection in the CRQE simulations remains unorganized, typically with several relatively shallow clouds present in the domain at any one time and occasionally deep convective towers developing at random locations and proceeding through their life cycle (i.e., from the development initially as one of the shallow clouds; deepening to reach the upper troposphere; to the termination, leaving an upper-tropospheric anvil remnant). For significantly larger computational domains (say, several tens of thousands of kilometers), one might expect the development of significant local vertical shear that supports organized convection, even if the domain-averaged wind is forced to be uniform (e.g.,

Grabowski and Moncrieff 2001, 2002). Such large-domain simulations might be a logical next step to investigate the indirect aerosol effects on various types of moist convection, including the organized convection. They would be especially worthwhile, considering the insignificant effects of aerosols on precipitation from the organized convection in simulations applying 2D kinematic framework (i.e., with the prescribed flow) reported in Slawinska et al. (2009).

Finally, the system dynamics (or cloud ensemble) approach applies to an area large enough to support many clouds and periods long enough to include many subsequent cloud life cycles. This implies that for a small area (say, a few hundreds kilometers) and periods of several hours, the process-level (or single cloud) thinking might provide a sensible paradigm. However, cloud processes within such a small area depend not only on internal processes (cloud, radiation, surface, among others) but the large-scale advective processes (i.e., the large-scale forcing) as well. Simulations using a limited-area domain and observationally derived large-scale forcing were performed in the past to investigate the impact of cloud microphysics on simulated clouds (e.g., Grabowski et al. 1999; Wu et al. 1999). Such simulations do provide useful insights into the possible effects of cloud microphysics, but their response is mostly determined by the imposed large-scale conditions. For instance, in the case of GATE cloud systems simulated in Grabowski et al. (1998), the response of simulated cloud systems was determined by the large-scale forcing and the large-scale horizontal wind field that forced changes between non-squall clusters, squall clusters, and scattered shallow convection. Cloud microphysics had a relatively small effect through the impact on surface processes and on upper-tropospheric anvil clouds. In particular, the mean (domain averaged) surface precipitation rate was virtually unaffected. This is similar to the situation with the boundary layer clouds for which Stevens and Brenguier (2009) argued that the large-scale effects overwhelm the effects of aerosols and separation of one from the other is extremely difficult.

Arguably, subtle modifications of the latent heating profiles [for instance, through the mechanism suggested by Rosenfeld et al. (2008)] can affect the large-scale circulation and impact the development of subsequent clouds. Such a chain of events can lead to either positive or negative feedback (i.e., either increased or reduced large-scale forcing) and can only be investigated in simulations that capture the range of scales from convective to the Rosby radius of deformation. For the nonrotating atmosphere like in the tropics, the upper bound implies planetary scale. It follows that the appropriate framework to investigate indirect effects of atmospheric aerosols on climate needs to cover at least four decades of horizontal scales. We hope to report on such simulations in the future.

5. Summary

This paper discusses the results from a series of simulations of convective–radiative quasi equilibrium (CRQE) over a surface with fixed characteristics (surface albedo of 0.15, surface temperature of 15°C, and relative humidity of 85%) and prescribed solar input (342 W m^{-2}), mimicking the mean conditions on earth (KT97). This study follows Grabowski (2006, hereafter G06). The new simulations feature sophisticated double-moment warm-rain and ice microphysics schemes (Morrison and Grabowski 2007, 2008a,b), which allow for a more realistic representation of the aerosol impact on precipitation processes and on the coupling between clouds and radiative transfer. Two aerosol characteristics were prescribed, referred to as PRISTINE and POLLUTED, and their impact was contrasted as in G06. The set of simulations directly following G06 was referred to as BASIC. In addition, four sets of sensitivity simulations were also performed that included (i) changes in the prescribed mean wind (increasing the wind from 4 to 8 m s^{-1}; set WIND8); changes in the surface characteristics [(ii) either reducing the surface relative humidity from 85% in BASIC to 75% in SRH75 or (iii) raising the surface temperature to 28°C with surface RH of 85% in ST28 to deepen the layer with warm-rain processes]; and (iv) replacing the double-moment rain scheme with the single-moment scheme (i.e., prescribing the raindrop size distribution intercept parameter; set MARPAL). These simulations provided either a context for the differences between the PRISTINE and POLLUTED cases in the BASIC set or helped to explain the differences between the BASIC set here and the simulations in G06.

In general, most results from the BASIC set are consistent with G06. The differences include slightly lower tropospheric water vapor content (which resulted in the smaller atmospheric radiative cooling) and smaller lower-tropospheric cloud fraction (which lead to smaller TOA albedo). These changes increased the net surface energy fluxes. The most significant difference from G06 was a large reduction of the difference between the PRISTINE and POLLUTED cases [e.g., with a range of ~(20–4) W m^{-2} at the surface], much larger than the simulated reduction of the lower-tropospheric cloud fraction would imply. The impact of the mixing scenario due to entrainment and mixing was also significantly smaller than in G06, ~2 W m^{-2}—that is, about half of the difference between PRISTINE and POLLUTED (in contrast to being as large as the 20 W m^{-2} (PRISTINE − POLLUTED) difference

in G06). At TOA, the difference between the PRISTINE and POLLUTED BASIC cases was ~9 W m^{-2}, with the difference between simulations with the same CCN characteristics and different mixing scenarios reduced to a mere 1 W m^{-2}. As in G06, the surface precipitation rate was approximately the same in PRISTINE and POLLUTED because it was controlled by the radiative cooling of the troposphere and the partitioning of the surface flux into sensible and latent components (i.e., the Bowen ratio), neither affected significantly by the CCN characteristics.

Increasing the mean wind (WIND8) or reducing the availability of water at the surface (SRH75) resulted in changes of the equilibrium state significantly larger than the difference between PRISTINE and POLLUTED in the BASIC set. The adjustments of the equilibrium states as well as energy and water fluxes across the atmosphere highlight the system dynamics (or cloud ensemble) reasoning and underscore the rather small impact of cloud microphysics. The key aspect is that the system dynamics approach incorporates the interactions (forcings and feedbacks) among all the relevant processes in the modeled system. For instance, increasing the wind in WIND8 leads to the increase of the total surface heat flux as implied by the process-level reasoning; however, the change is inconsistent with the imposed modifications because the mean surface wind almost doubled in WIND8, but the surface flux increased by a mere 12%. A simple explanation of the small surface flux increase in WIND8 is that the increase of the surface wind was accompanied by the increase of surface air temperature and humidity (i.e., the reduction of the surface and the air differences), so that the total surface heat flux matched the modified radiative cooling. In other words, the changes observed in WIND8 (and SRH75) were because of the increase in WIND8 (reduction in SRH75) of the atmospheric radiative cooling (due to changes of the atmospheric water vapor content), which required the appropriate adjustment of the total surface flux. In general, the indirect impact of aerosols on atmospheric processes appeared to be rather small when the system dynamics approach of CRQE is contrasted with the process-level reasoning.

An unexpected difference between G06 and BASIC simulations here is the partitioning of the total surface heat flux into latent and sensible components (the Bowen ratio). By applying a single-moment scheme for rain in the set MARPAL, it was shown that the change was mostly caused by the modification of the rain evaporation beneath the cloud base (i.e., in the boundary layer) in the double-moment-scheme results. The double-moment scheme predicted a significantly smaller rain evaporation rate, which resulted in a smaller mean temperature and a larger mean water vapor difference between the surface and the air near the surface. These changes between G06 and BASIC resulted in a significantly different surface flux Bowen ratio, ~0.25 in G06 and ~0.12 in BASIC. The impact of cloud microphysics on the quasi-equilibrium state through the boundary layer processes, the bottleneck connecting surface characteristics to the free atmosphere, may have far-reaching consequences for the clouds-in-climate problem. The differences between results from models applying single-moment and double-moment microphysics schemes (or even more complicated representations of raindrops spectra and thus rain evaporation) need to be put in the context of available observations, for instance, the magnitude and spatial variability of boundary layer temperature and moisture perturbations in convective situations. Such an investigation is underway and will be reported in future publications.

Acknowledgments. Part of this work was completed during WWG's visit to the French National Center for Meteorological Research (CNRM), Toulouse, supported by the CNRM's Research Visitor Fellowship. This work was also partially supported by the NOAA Grant NA08OAR4310543, DOE ARM Grant DE-FG02-08ER64574, and the NSF Science and Technology Center for Multiscale Modeling of Atmospheric Processes (CMMAP), managed by Colorado State University under Cooperative Agreement ATM-0425247. Constructive comments on the manuscript by three anonymous referees are also acknowledged.

REFERENCES

Andrejczuk, M., W. W. Grabowski, S. P. Malinowski, and P. K. Smolarkiewicz, 2009: Numerical simulation of cloud–clear air interfacial mixing: Homogeneous versus inhomogeneous mixing. *J. Atmos. Sci.,* **66,** 2493–2500.

Bigg, E. K., 1953: The supercooling of water. *Proc. Phys. Soc. London,* **B66,** 688–694.

Brown, A. R., and Coauthors, 2002: Large-eddy simulation of the diurnal cycle of shallow convection over land. *Quart. J. Roy. Meteor. Soc.,* **128,** 1075–1093.

Grabowski, W. W., 1998: Toward cloud resolving modeling of large-scale tropical circulations: A simple cloud microphysics parameterization. *J. Atmos. Sci.,* **55,** 3283–3298.

——, 2001: Coupling cloud processes with the large-scale dynamics using the cloud-resolving convection parameterization (CRCP). *J. Atmos. Sci.,* **58,** 978–997.

——, 2004: An improved framework for superparameterization. *J. Atmos. Sci.,* **61,** 1940–1952.

——, 2006: Indirect impact of atmospheric aerosols in idealized simulations of convective–radiative quasi equilibrium. *J. Climate,* **19,** 4664–4682.

——, and P. K. Smolarkiewicz, 1990: Monotone finite difference approximations to the advection–condensation problem. *Mon. Wea. Rev.,* **118,** 2082–2097.

——, and ——, 1999: CRCP: A cloud resolving convection parameterization for modeling the tropical convecting atmosphere. *Physica D,* **133,** 171–178.

——, and M. W. Moncrieff, 2001: Large-scale organization of tropical convection in two-dimensional explicit numerical simulations. *Quart. J. Roy. Meteor. Soc.,* **127,** 445–468.

——, and ——, 2002: Large-scale organization of tropical convection in two-dimensional explicit numerical simulations: Effects of interactive radiation. *Quart. J. Roy. Meteor. Soc.,* **128,** 2349–2375.

——, and J. C. Petch, 2009: Deep convective clouds. *Clouds in the Perturbed Climate System: Their Relationship to Energy Balance, Atmospheric Dynamics, and Precipitation,* J. Heintzenberg and R. J. Charlson, Eds., Strüngmann Forum Reports, Vol. 2, MIT Press, 197–215.

——, X. Wu, and M. W. Moncrieff, 1996: Cloud-resolving modeling of tropical cloud systems during phase III of GATE. Part I: Two-dimensional experiments. *J. Atmos. Sci.,* **53,** 3684–3709.

——, ——, ——, and W. D. Hall, 1998: Cloud-resolving modeling of cloud systems during phase III of GATE. Part II: Effects of resolution and the third spatial dimension. *J. Atmos. Sci.,* **55,** 3264–3282.

——, ——, and ——, 1999: Cloud resolving modeling of tropical cloud systems during phase III of GATE. Part III: Effects of cloud microphysics. *J. Atmos. Sci.,* **56,** 2384–2402.

——, and Coauthors, 2006: Daytime convective development over land: A model intercomparison based on LBA observations. *Quart. J. Roy. Meteor. Soc.,* **132,** 317–344.

——, O. Thouron, J.-P. Pinty, and J.-L. Brenguier, 2010: A hybrid bulk–bin approach to model warm-rain processes. *J. Atmos. Sci.,* **67,** 385–399.

Khairoutdinov, M., and Y. Kogan, 2000: A new cloud physics parameterization in a large-eddy simulation model of marine stratocumulus. *Mon. Wea. Rev.,* **128,** 229–243.

Kiehl, J. T., and K. E. Trenberth, 1997: Earth's annual global mean energy budget. *Bull. Amer. Meteor. Soc.,* **78,** 197–208.

——, J. J. Hack, and B. P. Briegleb, 1994: The simulated earth radiation budget of the National Center for Atmospheric Research community climate model CCM2 and comparisons with the Earth Radiation Budget Experiment (ERBE). *J. Geophys. Res.,* **99,** 20 815–20 827.

Meyers, M. P., P. J. DeMott, and W. R. Cotton, 1992: New primary ice-nucleation parameterizations in an explicit cloud model. *J. Appl. Meteor.,* **31,** 708–721.

Morrison, H., and W. W. Grabowski, 2007: Comparison of bulk and bin warm-rain microphysics models using a kinematic framework. *J. Atmos. Sci.,* **64,** 2839–2861.

——, and ——, 2008a: A novel approach for representing ice microphysics in models: Description and tests using a kinematic framework. *J. Atmos. Sci.,* **65,** 1528–1548.

——, and ——, 2008b: Modeling supersaturation and subgrid-scale mixing with two-moment bulk warm microphysics. *J. Atmos. Sci.,* **65,** 792–812.

——, G. Thompson, and V. Tatarskii, 2009: Impact of cloud microphysics on the development of trailing stratiform precipitation in a simulated squall line: Comparison of one- and two-moment schemes. *Mon. Wea. Rev.,* **137,** 991–1007.

Pruppacher, H. R., and J. D. Klett, 1997: *Microphysics of Clouds and Precipitation*. Kluwer Academic, 954 pp.

Rosenfeld, D., U. Lohmann, G. B. Raga, C. D. O. Dowd, M. Kulmala, S. Fuzzi, A. Reissell, and M. O. Andreae, 2008: Flood or drought: How do aerosols affect precipitation? *Science,* **321,** 1309–1313.

Slawinska, J., W. W. Grabowski, H. Pawlowska, and A. A. Wyszogrodzki, 2008: Optical properties of shallow convective clouds diagnosed from a bulk-microphysics large-eddy simulation. *J. Climate,* **21,** 1639–1647.

——, ——, and H. Morrison, 2009: Impact of atmospheric aerosols on precipitation from deep organized convection: A prescribed-flow modeling study using double-moment bulk microphysics. *Quart. J. Roy. Meteor. Soc.,* **135,** 1906–1913.

Solomon, S., D. Qin, M. Manning, M. Marquis, K. Averyt, M. M. B. Tignor, H. L. Miller Jr., and Z. Chen, Eds., 2007: *Climate Change 2007: The Physical Science Basis*. Cambridge University Press, 996 pp.

Stevens, B., and J.-L. Brenguier, 2009: Cloud-controlling factors: Low clouds. *Clouds in the Perturbed Climate System: Their Relationship to Energy Balance, Atmospheric Dynamics, and Precipitation,* J. Heintzenberg and R. J. Charlson, Eds., Strüngmann Forum Reports, Vol. 2, MIT Press, 173–195.

——, and G. Feingold, 2009: Untangling aerosol effects on clouds and precipitation in a buffered system. *Nature,* **461,** 607–613.

Troen, I., and L. Mahrt, 1986: A simple model of the atmospheric boundary layer: Sensitivity to surface evaporation. *Bound.-Layer Meteor.,* **37,** 129–148.

Wu, X., and M. W. Moncrieff, 1999: Effects of sea surface temperature and large-scale dynamics on the thermodynamic equilibrium state and convection over the tropical western Pacific. *J. Geophys. Res.,* **104** (D6), 6093–6100.

——, W. W. Grabowski, and M. W. Moncrieff, 1998: Long-term behavior of cloud systems in TOGA COARE and their interactions with radiative and surface processes. Part I: Two-dimensional modeling study. *J. Atmos. Sci.,* **55,** 2693–2714.

——, W. D. Hall, W. W. Grabowski, M. W. Moncrieff, W. D. Collins, and J. T. Kiehl, 1999: Long-term behavior of cloud systems in TOGA COARE and their interactions with radiative and surface processes. Part II: Effects of cloud microphysics on cloud–radiation interaction. *J. Atmos. Sci.,* **56,** 3177–3195.

Xu, K.-M., and Coauthors, 2002: An intercomparison of cloud-resolving models with the atmospheric radiation measurement summer 1997 intensive observation period data. *Quart. J. Roy. Meteor. Soc.,* **128,** 593–624.